SEMARAK ILMU PUBLISHING

CFD Letters

Journal homepage:
https://semarakilmu.com.my/journals/index.php/CFD_Letters/index
ISSN: 2180-1363

Heat Transfer Enhancement in Stirling Engines Using Fins with Different Configurations and Air Flow

Abdelrahman Gomaa[1], Abdullah Alsit[1], Sharul Sham Dol[1,*]

[1] Department of Mechanical Engineering, Faculty of Engineering, Abu Dhabi University, Abu Dhabi, UAE

ARTICLE INFO

Article history:
Received 19 June 2022
Received in revised form 19 July 2022
Accepted 19 August 2022
Available online 31 October 2022

Keywords:
Stirling engine; Fin efficiency; Turbulent flow; Convection; Heat transfer

ABSTRACT

The Stirling engine, in comparison to other classical engines, is an external enclosed heat engine cycle with extraordinary theoretical efficiency and minimal emissions. However, when combined with a minor heat source, the productivity of the Stirling engine suffers. Thus, this study emphasizes research on improving engine performance using heat transfer. A simulation was done using CFD analysis in ANSYS Fluent to enhance heat transfer using different types of fins, air blowers, and roughness. κ-ω SST model was used as the turbulence model to capture the heat transfer behavior near and away from the surface. All runs showed a higher heat transfer rate per unit area than the no finned case. Increasing the number of fins reduces the heat transfer by 10 %, Applying this solution would cost more since more material is needed to decrease the gap between fins. When doubling the length of the fin, the heat transfer of the circular design was reduced by 1%, the pinned design by 5%, and the squared design by 30%. The addition of fins reduced the flow of heat to the cold end and kept the temperature near the cold end below 100°C. Increasing the roughness resulted in a small increase in heat flow. Comparing the laminar flow to the transitional flow, the transitional flow increases the heat transfer by 1000%.

1. Introduction

If present energy consumption patterns continue, they may contribute to global warming. This occurrence is a severe environmental concern that emits enormous amounts of greenhouse gases [1,2]. The heat generated is heat that is rejected into the ambience although it may yet be reused for several meaningful and lucrative reasons. This includes excess heat discarded in the aviation sector. The strategy for recovering this heat is solely based on the temperature of the excess heat gases and the expenses implicated [3,4]. These increases in heat supplies created in our dwelling space may eventually boost the ambient temperature and might even contribute to global warming if not addressed appropriately. As a result, waste heat must be collected and repurposed as electric energy [5]. Present equipment captures and transforms this usually unusable waste heat to generate emission-free power, allowing industrial manufacturers to reinvest their squandered energy in the development that generated it. A considerable amount of research and development has gone into

* *Corresponding author.*
E-mail address: sharulshambin.dol@adu.ac.ae (Sharul Sham Dol)

https://doi.org/10.37934/cfdl.14.10.1631

these systems, which are capable of producing power from waste heat at minimal temperatures [6]. Because of the oscillating nature of the working fluid evolvement, studying the Stirling engine is extremely complicated [7]. Varied thermodynamic methods of the Stirling engine functioning with various assumptions have been proposed in the literature. The Stirling engine seems probable for harnessing the massive quantity of waste heat produced from manufacturing procedures and renewable thermal energy resources for producing electricity [8,9]. This engine is also projected to provide low-emission, noise-free power generation machines with exceptional fuel-saving and multifuel capacity [10, 11]. There are many limitations for the usage of Stirling engine. One of the main drawbacks of the Stirling engine is that it has a relatively low specific power (ratio of power to volume swept by the piston) when compared to I.C. engines. The Stirling engine's requirement for a specific amount of warming up time before it can begin to create power is another drawback. Moreover, a constant heat source It may be necessary to use special heat-resistant materials to construct the hot part of the engine due to its potentially hazardous temperature. The restricted space for heat transfer between the heat source and the working gas makes this engine more difficult to scale up. In fact, an excessively large engine will require too much space for an efficient heat transfer to the working gas [12]. As a result, scholars in energy-related disciplines have given the Stirling engine a lot of thought in recent years [13]. The main objective of this paper is to find the difference between the no finned Stirling engine and the different configurations using CFD analysis in ANSYS Fluent. The proposed configurations in this paper are the addition of extra surface area with a different geometric configuration, changing the material roughness and applying air flow over the Stirling engine using blowers. All the geometric enhancement on the fin design and other technique used to enhance the heat transfer rate can be applied on other stirling engins types.

1.1 Beta Type Stirling Engine

The configuration of the piston engine, heat exchangers, and displacer in a single cylinder of very robust glass was studied in a beta-type Stirling engine. A cyclical alternate motion with an angle of 110 is performed by the two pistons. It can function like an engine through employing an electrical resistance at the peak of the cylinder as the cause of heat [14]. The displacer pushes the air to go from the base to the top of the cylinder and conversely. Figure 1 depicts the investigated hot air engine arrangement [15]. The working fluid is supposed to be air, which behaves as an ideal gas. It may operate as an engine and offer mechanical energy, or as refrigerating machinery (inverse cycle), making dismantling simple. Because the pressure load is one bar and should stay one bar, this engine produces very little mechanical power [16]. The working fluid occupies three regions in the engine: the hot region, the cold region, and the regenerator region. The hot volume is located over the displacer head. The cold volume is located between the piston upper and the displacer bottom. The beta design has both pistons in the same engine housing and the same axial direction. The beta design enables the piston strokes to overlap for a portion of the cycle. This minimizes total engine area while increasing pressure swing without reducing operating areas [17]. The gamma configuration partially solves the beta configuration's centring problem. The beta variant has been widely utilized with excellent performance outcomes, and it was also the earliest Free piston Stirling engine (FPSE) to be built. To reduce vibrations, two beta configuration engines may be readily joined to work horizontally faced [18].

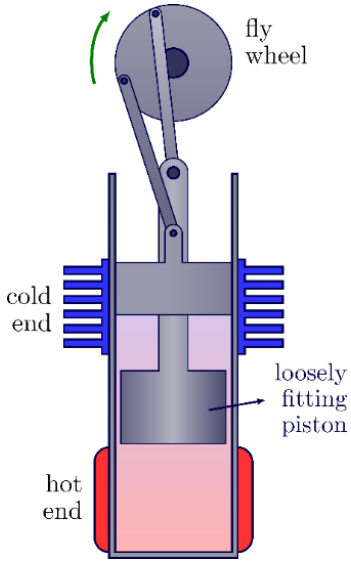

Fig. 1. Diagram of the β - type Stirling engine [15]

1.2 Kinematic and Free Piston

The kinematical relationships are used to compute hot and cold volumes. The kinematic relationships and schematic representation of the engine further with the rhombic-drive mechanism are shown in Figure 2. The regenerator area is the space between the displacer's outside and inside surfaces, and it has a constant amount [19]. For Stirling engines, the simultaneous motion of the piston and displacer, known as the phase, is critical for ensuring the position of the working fluid. If the piston and displacer are not in phase, the Stirling engine delivers no energy. The phase of a kinematic engine is determined by mechanically connecting the piston and displacer to a rotary motion and flywheel. The free-piston sterling engine does this by substituting the crank mechanism with a linear storing tool connected to both the piston and the displacer. As a result, the piston and displacer get decoupled [20].

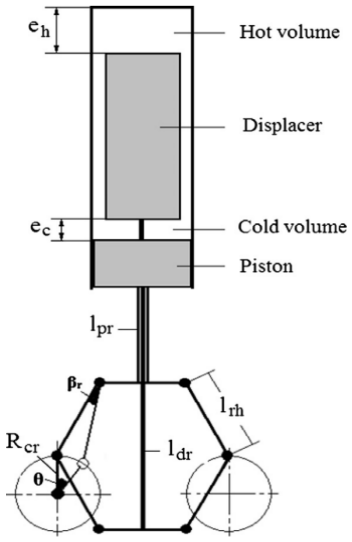

Fig. 2. Schematic view of the engine [21]

A linear storage device functions exclusively in the path of the piston or displacer movement, with no surface forces. A linear storage machine can be a compression spring, a gas spring, or a flexure bearing. Figure 3 depicts a schematic comparison. Cheng and Yang (2012) further demonstrated that the performance of a kinematic Stirling engine is greatly reliant on mechanism effectiveness [21]. For example, as the mechanism effectiveness was enhanced from 0.7% to 0.8%, the highest dimensionless shaft load practically doubled. The mechanism effectiveness in a free-piston design is essentially 1 [22].

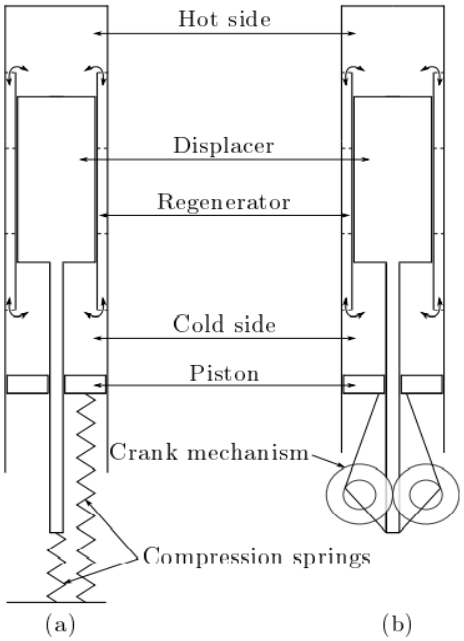

Fig. 3. Stirling engine comparison. (a) Free-piston Stirling engine, (b) Kinematic Stirling engine [18]

1.3 Cycle Study

Cycle analysis is a perfect representation of what happens in a Stirling engine and is therefore never utilized alone. It serves as the foundation for other approaches, particularly second-order approaches. The ideal Stirling cycle, ideal isothermal model, and ideal adiabatic model are the three cycles employed.

1.3.1 Ideal stirling cycle

Ideal Stirling cycle was developed for internal combustion engines to represent the mathematical thermodynamic cycle that the working fluid goes through. It is assumed that all working fluids follow an identical set of procedures. Figure 4 depicts the ideal Stirling cycle, which consists of four processes [23]. However, the cycle of the Stirling engine is not the sole cycle with an efficiency equivalent to the efficiency of the Carnot cycle. The Stirling cycle and the Carnot cycle are both parts of the Reitlinger cycle, which is made up of two isothermal and two polytropic procedures of the same type. Nevertheless, it will be more complicated to have heat into bigger Stirling engines. The volume of working fluid rises quadratically as the radius of the Stirling engine rises, whereas the heat transfer

space to the working fluid only grows linearly. The Stirling cycle is therefore reduced to the Otto cycle, often known as the adiabatic Stirling cycle [24].

1.3.2 Schmidt model

Because the Stirling engine contains multiple temperature zones, not all the working fluid goes through the identical thermodynamic cycle. The Schmidt model was developed by considering that each of the five primary engine areas, including the compression zone, cooler, heater, regenerator, and expansion area, is isothermal. The compression and cooler are at heat sink temperature T_{cold}, whereas the heater and expansion area are at heat source temperature T_{hot}. The design then carries on to account for volume variations in the compression and expansion areas by presuming sinusoidal movement with a phase difference among both. Because all of the sectors are isothermal, the Schmidt model is also known as the isothermal model. The Schmidt model's statements are summarized in this way: a) known temperatures for the engine's various compartments, b) sinusoidal movement of components, c) working fluid is an ideal gas, d) constant mass of working fluid, e) pressure is constant throughout the engine [25]. A significant finding is the generation of a pressure formula that is specified for the whole cycle. The pressure formula yields the following results:

$$P = \frac{M.R}{\left(\frac{V_h}{T_h}\right)+\left(\frac{V_r}{T_r}\right)+\left(\frac{V_c}{T_c}\right)} \tag{1}$$

Just the effective regenerator temperature (T_r) should be expressed in T_{hot} and T_{cold} forms. The regenerator's length (L_r) is presumed to have a linear temperature distribution, which is integrated with relation to mass along its length and then contrasted to the ideal gas formula as follows:

$$T_r(x) = \frac{T_h - T_c}{L_r} x + T_c \tag{2}$$

$$m_r = \frac{PV}{RT_{eff}} \tag{3}$$

$$T_{eff} = \frac{T_h - T_c}{\ln\left(\frac{T_h}{T_c}\right)} \tag{4}$$

While there is no theoretical approach for determining the work done each cycle, a Fourier series extension of the pressure phrase can resolve the problem.

1.4 Governing Equations

The turbulence model was adopted since the flow in a combustion engine is often turbulent. Furthermore, if the design is in 3D, a turbulent flow method is preferable. Furthermore, in our situation, the cylinder design we created has a limited capacity between the boundary and the displacer, hence the flow is essentially turbulent in this region. The surface roughness of the cylinder and displacer could also contribute to the flow becoming turbulent. Navier Stokes models were utilized to resolve the formulas of transports including heat transfer and flow field within the cylinder [26]. These equations can be written as Eq. (5) to (10):

Continuity equation:

$$\frac{\partial \rho_f}{\partial t} + \frac{\partial}{\partial x}\left(\rho_f . \tilde{u}\right) + \frac{1}{r} . \frac{\partial}{\partial r}\left(\rho_f . r\tilde{v}\right) = 0 \quad (5)$$

x-momentum equation:

$$\frac{\partial}{\partial t}\left(\rho_f . u\right) + \frac{\partial}{\partial x}\left(\rho_f . \tilde{u}u\right) + \frac{1}{r} . \frac{\partial}{\partial r}\left(\rho_f . r\tilde{v}u\right) = \rho_f g - \frac{\partial P}{\partial x} + \mu . \frac{\partial}{\partial x}\left(\frac{\partial u}{\partial x}\right) + \frac{u}{r} . \frac{\partial}{\partial r}\left(r . \frac{\partial u}{\partial x}\right) + \frac{\mu}{3} . \frac{\partial}{\partial x}(\nabla . V) \quad (6)$$

y-momentum equation

$$\frac{\partial}{\partial t}\left(\rho_f . v\right) + \frac{\partial}{\partial x}\left(\rho_f . \tilde{u}v\right) + \frac{1}{r} . \frac{\partial}{\partial r}\left(\rho_f . r\tilde{v}v\right) = -\frac{\partial P}{\partial x} + \mu . \frac{\partial}{\partial x}\left(\frac{\partial v}{\partial x}\right) + \frac{u}{r} . \frac{\partial}{\partial r}\left(r . \frac{\partial v}{\partial x}\right) + \frac{\mu}{3} . \frac{\partial}{\partial r}(\nabla . V) - \frac{\mu v}{r^2} \quad (7)$$

Fluid energy equation:

$$\frac{\partial}{\partial t}\left(\rho_f . T_f\right) + \frac{\partial}{\partial x}\left(\rho_f . \tilde{u}T_f\right) + \frac{1}{r} . \frac{\partial}{\partial r}\left(\rho_f . r\tilde{v}T_f\right) = \frac{1}{c_{pf}}\left[\frac{\partial P}{\partial t} + \nabla . pV - p(\nabla . V)\right] + \frac{k_f}{C_{Pf}}\left[\frac{\partial}{\partial x}\left(\frac{\partial T_f}{\partial x}\right) + \frac{1}{r} . \frac{\partial}{\partial r}\left(r . \frac{\partial T_f}{\partial r}\right)\right] + \frac{2\mu}{C_{pf}}\left[\left(\frac{\partial u}{\partial x}\right)^2 + \left(\frac{\partial r}{\partial r}\right)^2 + \left(\frac{v}{r}\right)^2\right] + \left(\frac{\partial v}{\partial x} + \frac{\partial u}{\partial r}\right)^2 \left(\frac{2}{3}(\nabla . V)\right)^2 \quad (8)$$

Solid energy equation:

$$\frac{\partial}{\partial t}\left(\rho_s . T_s\right) = \left(k_s / C_{ps}\right)\left[\frac{\partial}{\partial x}\left(\frac{\partial T_s}{\partial x}\right) + \frac{1}{r} . \frac{\partial}{\partial r}\left(r . \frac{\partial T_s}{\partial r}\right)\right] \quad (9)$$

Ideal gas Equation:

$$PV = \rho_f R T_f \quad (10)$$

T_s denotes the solid temperature and T_f is the fluid temperature. $\tilde{u}$ and $\tilde{v}$ are the relative velocity elements among both fluid and mobile frames. The k - ε realizable turbulence model, Eq. (11) and (12), with typical wall functions are utilized to construct this set of equations [27]. In the examined fluid flow and heat transfer analysis, the selected model fulfils the accuracy and reliability requirements.

k-equation (Turbulent kinetic energy):

$$\frac{\partial}{\partial t}(\rho k) + \frac{\partial}{\partial x_i}(\rho k u) + \frac{\partial}{\partial x_i}(\rho k v) + \frac{\partial}{\partial x_i}(\rho k w) = \frac{\partial}{\partial x_j}\left(\frac{\mu_t}{\sigma_k} . \frac{\partial k}{\partial x_j}\right) - \rho\varepsilon + 2\mu_t E_{ij} . E_{ij} \quad (11)$$

ε-equation (dissipation of the turbulent kinetic energy):

$$\frac{\partial}{\partial t}(\rho\varepsilon) + \frac{\partial}{\partial x_i}(\rho\varepsilon u) + \frac{\partial}{\partial x_i}(\rho\varepsilon v) + \frac{\partial}{\partial x_i}(\rho\varepsilon w) = \frac{\partial}{\partial x_j}\left(\frac{\mu_t}{\sigma_\varepsilon} . \frac{\partial \varepsilon}{\partial x_j}\right) + C_{1\varepsilon}\left(2\mu_t E_{ij} . E_{ij}\right) . \frac{\varepsilon}{k} - C_{2\varepsilon}\rho . \frac{\varepsilon^2}{k} \quad (12)$$

The ideal gas model was utilized to compute density, while the kinetic theory was applied to estimate heat capacity and viscosity. Consequently, neither viscous heating nor gravity factors were considered in this study. The ideal gas formula is employed to establish the value of pressure since

the pressure difference produced by gas flow within the engine is only a minor proportion of the total amount of pressure [28].

2 Methodology

The solution methodology between both cases is almost the same. except in turning the gravity effect on for cases where air flow is present. The energy model is turned on followed by using the $\kappa - \omega$ SST model. The SST $\kappa - \omega$ model was created to syndicate the $\kappa - \varepsilon$ model's robust and precise formulation in the near-wall region with the k model's freestream independence in the distant field. The $\kappa - \varepsilon$ model is transformed into a $\kappa - \omega$ formulation to achieve this. A blending function is applied to multiply the standard $\kappa - \omega$ model with the altered $\kappa - \varepsilon$ model, and then both models are added together. The blending function is established to one in the near-wall region, triggering the regular $\kappa - \omega$ model, and zero away from the surface, triggering the transformed $\kappa - \varepsilon$ model [29].

The continuity, energy, and momentum equations in this case were solved using Ansys Fluent. To discretize the differentials, the program uses the finite volume method. Because it promotes precision, the second order upwind finite scheme was adopted [30]. Coupled solver was used because it provides an accurate result compared to others.

2.1 Geometry Description

Fusion 360 was used to create a three-dimensional domain. The domain is split into five sections: the hot end, cold end, displacer, cover, and environment. For both the finned and the no finned cases, the domain was designed to be modelled quarterly to lower the overall number of elements and computer resources required. Figure 4 shows the schematic drawing of the Stirling engine and the dimensions in Table 1. The heated end was first drawn, based on the dimensions obtained from many resources, by sketching a cylinder and vertically dividing it into four equal halves: then, eliminating three of the four parts. The hot end was then duplicated to represent the cool end. After that, the displacer, which joins the hot end and the cold end, is drawn. Finally, the cover and the surrounding environment were drawn. Additionally, for the finned design, the fins were placed to cover the whole area from the cold end to the displacer, to maximize the difference in temperature between the cold end and the hot end as shown in Figure 5a. The regenerator was not consider in the design since the study is on the effect of fins on the Stirling engine. After drawing the model on fusion 360, the model was imported into Design Modeler to make the hot end, cold end, and displacer as one part to eliminate the interfaces between them. Figure 5 shows different fins types; squared fins, pinned fins, and circular fins.

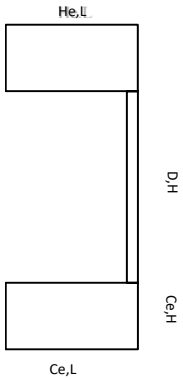

Fig. 4. Drawing Scheme

Table 1
Stirling engine design parameters

Part Name	Dimension (in mm)
He, L	19
He, H	16
D, H	78
D, L	1
Ce, H	16
Ce, L	19

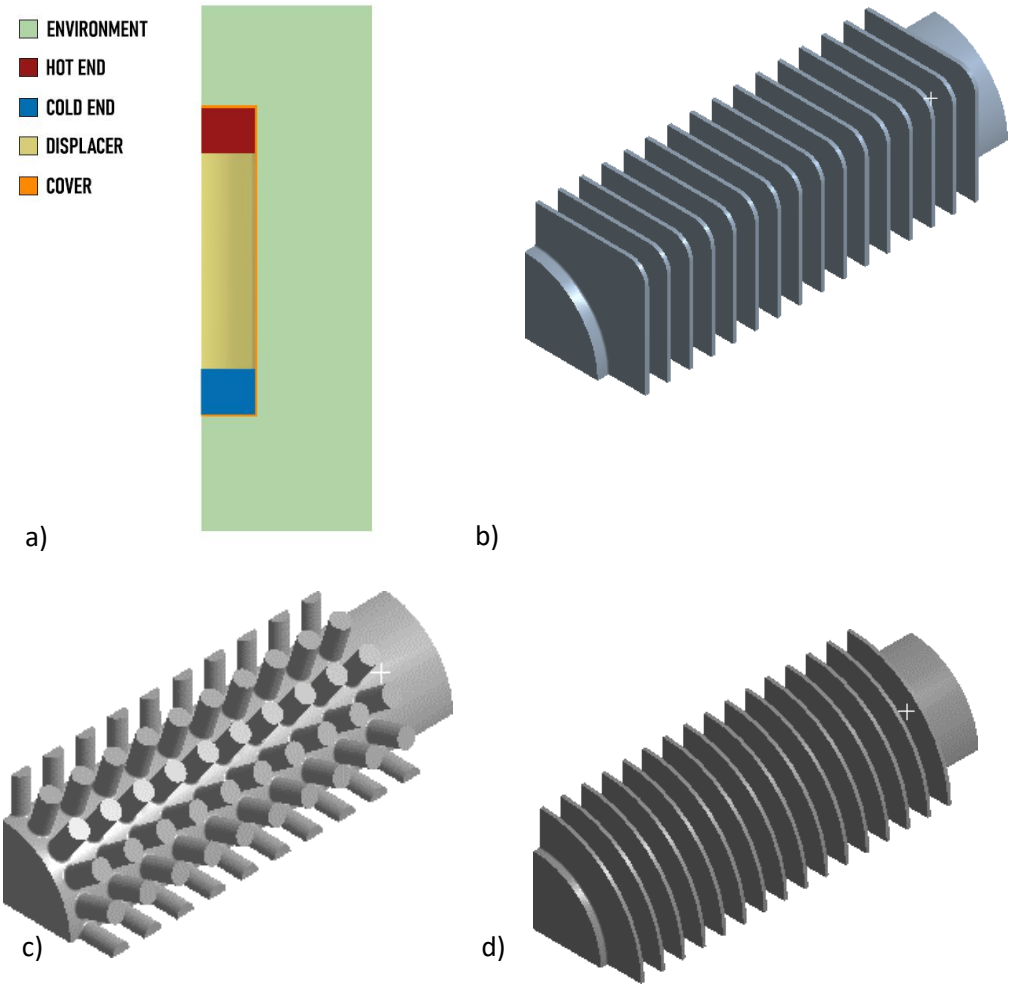

Fig. 5. a) Geometry Design b) squared fins design c) pinned fins design d) circular fins design

2.2 Mesh

Creating the mesh is the next critical step as it has a significant impact on the correctness of the outcomes. The mesh should be refined and aligned at the interfaces between the fluid and the solid bodies to have a reasonable heat flow. There are many components to be considered when determining the mesh for this situation. *y+* is one of the most critical components in increasing or decreasing the accuracy of the results, since high *y+* values near the wall boundaries will not have the ability to capture the behaviors near the wall. Moreover, the aspect ratio, skewness and orthogonal quality was used to determine the mesh quality [31]. After conducting the *y+* calculations using the following:

$$y^+ = \frac{Y\rho u_T}{\mu} \tag{13}$$

where *Y* is the first layer height, μ is the fluid viscosity, ρ is the fluid density and u_T is the friction velocity that can be calculated using the following:

$$u_T = \sqrt{\frac{\tau_W}{\rho}} \tag{14}$$

Where τ_W is the wall shear stress calculated by:

$$\tau_W = \mu \left.\frac{du}{dy}\right|_{y=0} \tag{15}$$

After conducting these calculations, the first layer height is $4e^{-5}$ m for a speed of 2 m/s and the 3e-6 for the 100 m/s. It was not possible to apply inflation layers in the finned cases, thus the mesh was refined near the wall to capture the behavior near the wall. Several mesh trails were conducted, and the simulation's results were judged based on the heat flux. The trials were made at 100000 elements, 400000 elements and 600000 elements as shown in Figure 6, the results showed the heat flux values were 0.7 kWm^{-2}, 0.585 kWm^{-2} and 0.58 kWm^{-2}.

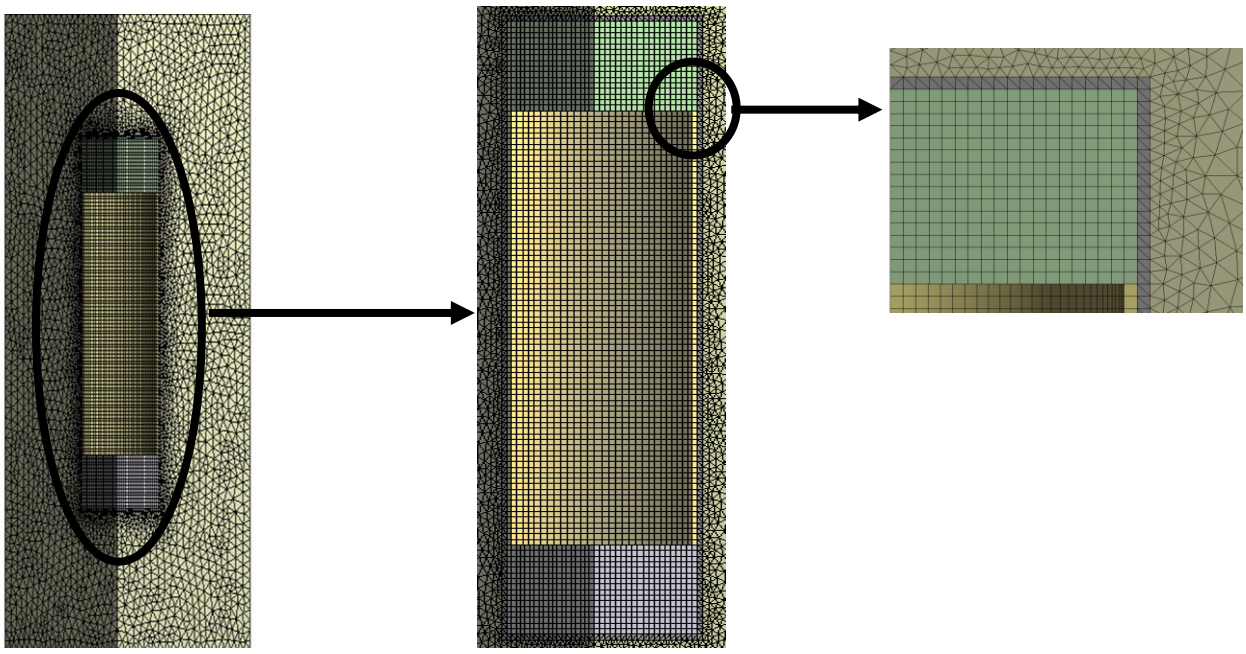

Fig. 6. Mesh

2.3 Boundary Conditions

All the parts are set to a fluid and selected material was air, except for the cover it was set solid and selected material is steel. Using the fixed value feature, the temperature of the hot end and the cold end are fixed at 800°C and 25°C correspondingly as shown in Figure 7. Afterwards, the interfaces between bodies are set to couple to allow the heat transfer through boundaries and a convection boundary condition is set at the outer surface of the cover with a heat transfer coefficient of 20 $\mathrm{Wm^{-2}K^{-1}}$.

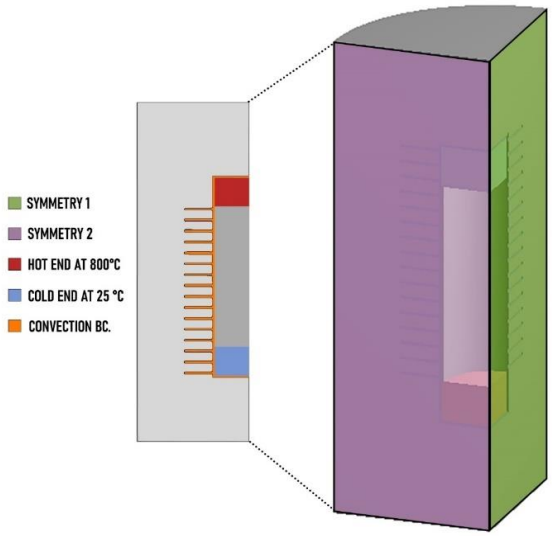

Fig. 7. Boundary Conditions

3. Results

In this section, the findings of the project will be discussed. Several simulations have been run to determine the impact of alternative fin attachments on the Stirling engine's power output and, ultimately, efficiency. The heat transfer rate attained by the Stirling engine model with no fins, circular fins, pin fins, and rectangular fins is displayed. In the case, while the Stirling engine is static, all possible cases were simulated to find how each change in the geometry and other features affected the rate of heat transfer in the model.

3.1 Natural Convection Case

All runs showed a higher heat transfer rate per unite area than the no finned case which had a value of 0.58 kWm^{-2}. According to Table 2, the results show that increasing the number of fins didn't enhance the heat transfer, but it reduced it by 10 %, Applying this solution would cost more since more material is needed to decrease the gap between fins. Moreover, doubling the length of the fin, compared to the default design, decreased by 1% in the circular design, 5% for the pinned design and 30% for the squared design. This can be due to reaching the ambient temperature at the fin tip which makes it hard to maintain the fin surface temperature at the base temperature. However, increasing the thickness of the fin showed an increase in the heat transfer rate due to the increase in the surface area of the fin, but using this solution would increase the cost compared to the default case.

Table 2
Heat Flux Results

Pinned Design		Circular Design		Squared Design	
Case	Heat flux in KWm^{-2}	Case	Heat flux in KWm^{-2}	Case	Heat flux in KWm^{-2}
5 mm spacing (default)	1.1	5 mm spacing (default)	0.751	5 mm spacing (default)	.983
2.5 mm spacing	1	2.5 mm spacing	0.671	2.5 mm spacing	0.925
Double Length	1.039	Double Length	0.742	Double Length	0.756
Double thickness	1.12	Double thickness	0.851	Double thickness	1.141

According to Table 3, It is clearly shown how the change in geometry affected the efficiency and the effectiveness of the fins. These results show how each case performs. It can be concluded that the double thickness design had the largest efficiency followed by the 5 mm spacing, then the 2.5 mm case and lastly the double-length case.

Table 3
Effectiveness Results

Pinned Design		Circular Design		Squared Design	
Case	Effectiveness	Case	Effectiveness	Case	Effectiveness
5 mm spacing (default)	1.9	5 mm spacing (default)	1.29	5 mm spacing (default)	1.69
2.5 mm spacing	1.72	2.5 mm spacing	1.16	2.5 mm spacing	1.59
Double Length	1.79	Double Length	1.28	Double Length	1.3
Double thickness	1.93	Double thickness	1.47	Double thickness	1.97

According to Figure 8, the no finned case had the highest temperature around the cold, which with time it will affect the performance of the Stirling engine by reducing the temperature difference between the hot end and the cold end. Adding fins decreased the flow of heat to the cold end and kept the area around the cold end below 100°C. This addition will help to keep the difference between the hot end and the cold end, and it will require more time to heat the area around the cold end.

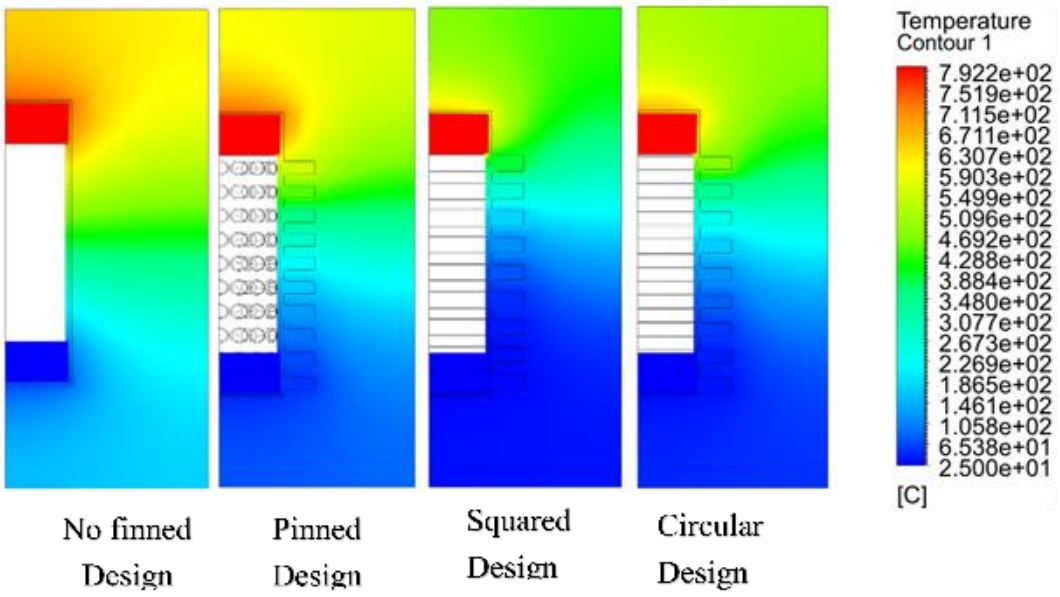

Fig. 8. Temperature Distribution

3.1.1 Theoretical calculations

The theoretical calculations done for the efficiencies of the fins, there are 3 types of the geometry, and each type has 4 different configurations, for the pinned fins we use these equations:
Pinned fins

$$\eta = \frac{tanh(mL)}{mL} \tag{16}$$

$$m = \sqrt{\frac{4h}{kD}} \tag{17}$$

$$L_c = L + \frac{D}{2} \tag{18}$$

Squared fins

$$\eta = \frac{tanh(mL)}{mL} \tag{19}$$

$$m = \sqrt{\frac{2h}{kt}} \tag{20}$$

$$L_c = L + \frac{t}{2} \tag{21}$$

Circular fins

$$\zeta = L_c^{\frac{3}{2}} \left(\frac{h}{kA_p}\right)^{\frac{1}{2}} \tag{22}$$

$$A_p = L_c t \tag{23}$$

$$L_c = L + \frac{t}{2} \tag{24}$$

Table 4 shows the results for the calculated efficiencies, it is noticed that the pinned fins have in general a higher efficiency among other fins, however, the highest efficiency value came up to be the double thickness squared fins.

Table 4
Fins Efficiencies Results

Pinned Design		Circular Design		Squared Design	
Case	Efficiency	Case	Efficiency	Case	Efficiency
5 mm spacing (default)	96 %	5 mm spacing (default)	91 %	5 mm spacing (default)	91.7 %
2.5 mm spacing	96 %	2.5 mm spacing	91 %	2.5 mm spacing	91.7%
Double Length	87.2 %	Double Length	68 %	Double Length	75.3%
Double thickness	97 %	Double thickness	96 %	Double thickness	97.5%

3.2 Forced Convection Case

In the case of static forced convection, the flow of air was applied at two different temperatures and velocities, also the material roughness was changed to see how the heat transfer rate will be affected. For the laminar case, a velocity of 2 m/s was applied at the inlet. By fitting in number into the Reynolds number equation and assuming the case as external flow, the result is 14000 which is less than $5e^5$. For the transition case, the velocity was set to 100 m/s, the result is $7e^5$ which is greater than $5e^5$ and less than $10e^7$. According to the below table 5. The simulations showed that changing

the surface roughness and applying airflow increased the heat flux by approximately 2800% and more. This phenomenon can be explained by using the Newton's law of cooling:

$$\dot{Q} = h(T_s - T_\infty) \tag{25}$$

Heat transfer is assisted by fluid motion, the higher the velocity, the faster the heat transfer rate [32]. The convective heat transfer coefficient h is greatly influenced by fluid characteristics, solid surface roughness, and fluid flow type (laminar or turbulent). The circular fins were chosen to be simulated under a flow of air as shown in Table 5, increasing the roughness showed a slight increase in the heat flux compared to the case with a smooth surface and increasing the temperature of the air blew reduced the heat flux compared to cases where the air was blown at a low temperature. This is because the change in T_s and T_∞ became smaller. Comparing the laminar flow cases to the turbulent flow cases, the turbulent flow cases showed an increase by approximately 10 times, since the turbulence is higher in the transitional flow compared to the laminar. In a turbulent flow, in addition to Molecular diffusion, fluctuations provide a second mechanism for heat transmission. These variations cause the eddies. These eddies quickly transmit mass, momentum, and energy across the flow [33]. Molecular diffusion is a slow process compared to eddies, and it is sometimes ignored when evaluating the heat transfer rate in turbulent flows. As a result, turbulent flows have a larger heat transfer coefficient than laminar flows [34].

Table 5
Air Flow and Roughness Results

Laminar flow		Transitional flow	
Case	Heat flux in KWm^{-2}	Case	Heat flux in KWm^{-2}
Smooth, 2 m/s 426 C air flow	29	Smooth, 100 m/s 426 C air flow	318.2
Smooth 2m/s 25c air flow	60.1	Smooth 100 m/s 25c air flow	663.2
rough, 2 m/s 426 C air flow	29.8	rough, 100 m/s 426 C air flow	319.8
rough, 2 m/s 25 C air flow	61.8	rough, 100 m/s 25 C air flow	664.3

In Figure 9, the difference in temperature distribution can be seen and how the laminar and the transitional flow cases differ from each other. In the laminar case, the air has more time to get in contact with the hot body, thus, we can see that the temperature of the air below the fins is almost 700 °C and above. In the turbulent case, the air has less time to get in contact with the body as a result the temperature under the fins is almost 300 °C.

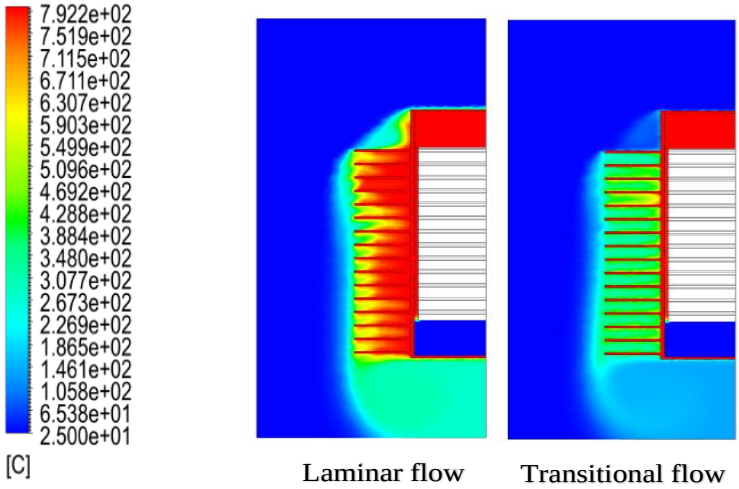

Fig. 9. Laminar and Transitional temperature Contours

3.3 Fan Calculation

This section shows the power consumption and the total cost needed to set a flow on the engine to increase the heat flux. We will start by determining the size of the fan needed. According to the dimensions, the fan dimension should be more than 19 mm in diameter.

For the 2 m/s case:

Thus, the dimension of the fan used is 25 mm by 25 mm by 10 mm. The next step is finding the power usage of the fan, which is calculated using the following:

$$P = VI \tag{26}$$

Where P is the Power in W; V is the fan's voltage, and I is the current in A. In our case:

$$P = 12(V) * 0.2(A) \tag{27}$$

$$P = 2.4\,W \cong 0.0024\,KW \tag{28}$$

The fan is assumed to work for 30 minutes to get the same results and try to enhance the heat transfer rate.

$$P * t = 0.0024(KW) * 0.5(h) \cong 0.0012\,KWh \tag{29}$$

For the 100 m/s air speed, it will require much bigger fan with nozzle and that will cost more than the 2 m/s case.

4. Conclusions

In this paper, a three-dimensional cylinder model of a Stirling engine with beta-type is simulated to improve the heat transfer rate and, as a result, the engine efficiency. The model is altered by adding various fins to the engine wall. Circular fins, pinned fins, and squared fins are used in CFD simulations and various geometry changes were applied to the fins such as changing the length, thickness and spacing. In most cases, the pinned fins had the highest heat transfer rate, except in increasing the thickness. Comparing the addition of the fins to the no finned Stirling engine, the heat flux value increased when the fin was added thus the efficiency increased. Also, Airflow and increasing the surface roughness were set as another addition. The findings demonstrated that using both ways improved heat flux values compared to the no-finned engine. The efficiency of the Stirling engine increased by 2800% when these additions were applied to the engine.

Acknowledgement
This research was not funded by any grant

References

[1] Saadon, Syamimi, Leon Gaillard, Stéphanie Giroux, and Christophe Ménézo. "Simulation study of a naturally ventilated building integrated photovoltaic (BIPV) envelope." *Energy Procedia* 78 (2015): 2004-2009. https://doi.org/10.1016/j.egypro.2015.11.394

[2] Dol, Sharul Sham, Abid Abdul Azeez, Mohammad Sultan Khan, Abdulqader Abdullah Hasan, and Mohammed Alavi. "Potential of Offshore Renewable Energy Applications in the United Arab Emirates." In *Clean Energy Opportunities in Tropical Countries*, pp. 237-265. Springer, Singapore, 2021. https://doi.org/10.1007/978-981-15-9140-2_12

[3] Dadi, Mohsin J., I. M. Molvi, and A. V. Mehta. "The most efficient waste heat recovery device: A gamma type stirling engine." *International journal of advanced engineering technology* 3, no. 5 (2012): 189-195.

[4] Azimov, Ulugbek, Eiji Tomita, Nobuyuki Kawahara, and Sharul Sham Dol. "Combustion characteristics of syngas and natural gas in micro-pilot ignited dual-fuel engine." *International Journal of Mechanical and Mechatronics Engineering* 6, no. 12 (2012): 2863-2870.

[5] Shih, Hua-Ju. "An analysis model combining gamma-type stirling engine and power converter." *Energies* 12, no. 7 (2019): 1322. https://doi.org/10.3390/en12071322

[6] Jouhara, Hussam, Navid Khordehgah, Sulaiman Almahmoud, Bertrand Delpech, Amisha Chauhan, and Savvas A. Tassou. "Waste heat recovery technologies and applications." *Thermal Science and Engineering Progress* 6 (2018): 268-289. https://doi.org/10.1016/j.tsep.2018.04.017.

[7] Buliński, Zbigniew, Ireneusz Szczygieł, Adam Kabaj, Tomasz Krysiński, Paweł Gładysz, Lucyna Czarnowska, and Wojciech Stanek. "Performance analysis of the small-scale α-type Stirling engine using computational fluid dynamics tools." *Journal of Energy Resources Technology* 140, no. 3 (2018). https://doi.org/10.1115/1.4037810

[8] Saadon, S. "Possibility of Using Stirling Engine as Waste Heat Recovery–Preliminary Concept." In *IOP Conference Series: Earth and Environmental Science*, vol. 268, no. 1, p. 012095. IOP Publishing, 2019. https://doi.org/10.1088/1755-1315/268/1/012095

[9] Almajri, Ahmad K., Saad Mahmoud, and Raya Al-Dadah. "Modelling and parametric study of an efficient Alpha type Stirling engine performance based on 3D CFD analysis." *Energy conversion and management* 145 (2017): 93-106. https://doi.org/10.1016/j.enconman.2017.04.073

[10] Thombare, D. G., and S. K. Verma. "Technological development in the Stirling cycle engines." *Renewable and Sustainable Energy Reviews* 12, no. 1 (2008): 1-38. https://doi.org/10.1016/j.rser.2006.07.001

[11] Alfarawi, Suliman, Raya Al-Dadah, and Saad Mahmoud. "Potentiality of new miniature-channels Stirling regenerator." *Energy conversion and management* 133 (2017): 264-274. https://doi.org/10.1016/j.enconman.2016.12.017

[12] Kongtragool, Bancha, and Somchai Wongwises. "A review of solar-powered Stirling engines and low temperature differential Stirling engines." *Renewable and Sustainable energy* reviews 7, no. 2 (2003): 131-154. https://doi.org/10.1016/S1364-0321(02)00053-9

[13] Yang, Hang-Suin, and Chin-Hsiang Cheng. "Development of a beta-type Stirling engine with rhombic-drive mechanism using a modified non-ideal adiabatic model." *Applied energy* 200 (2017): 62-72. https://doi.org/10.1016/j.apenergy.2017.05.075

[14] Dobre, Cătălina, Lavinia Grosu, Monica Costea, and Mihaela Constantin. "Beta type Stirling engine. schmidt and finite physical dimensions thermodynamics methods faced to experiments." *Entropy* 22, no. 11 (2020): 1278. https://doi.org/10.3390/e22111278

[15] Della Torre, Augusto, Andrea Guzzetti, Gianluca Montenegro, Tarcisio Cerri, Angelo Onorati, and Fethi Aloui. "CFD modelling of a beta-type Stirling machine." In *11th World Congress on Computational Mechanics, WCCM 2014, 5th European Conference on Computational Mechanics, ECCM 2014 and 6th European Conference on Computational Fluid Dynamics, ECFD 2014*, pp. 1096-1113. 2014. https://doi.org/10.13140/2.1.4560.7041

[16] Lottmann, Matthias, Zachary de Rouyan, Linda Hasanovich, Steven Middleton, Michael Nicol-Seto, Connor Speer, and David Nobes. "Development of a 100-Watt-Scale Beta-Type Low Temperature Difference Stirling Engine Prototype." In *E3S Web of Conferences*, vol. 313, p. 08004. EDP Sciences, 2021. https://doi.org/10.1051/e3sconf/202131308004

[17] Abed, Hayder M., and Yaseen H. Mahmood. "Fabrication of Stirling Engine and study its characteristics." *Tikrit Journal of Pure Science* 23, no. 8 (2018): 96-100.

[18] Paul, Christopher J., and Abraham Engeda. "Modeling a complete Stirling engine." *Energy* 80 (2015): 85-97. https://doi.org/10.1016/j.energy.2014.11.045

[19] Ridha, Alliche, Announ Mohamed, Chetti Boualem, and Kermezli Tayeb. "Two-Dimensional CFD Simulation Coupled with 6DOF Solver for analyzing Operating Process of Free Piston Stirling Engine." *Journal of Advanced Research in Fluid Mechanics and Thermal Sciences* 55, no. 1 (2019): 29-38.

[20] Deetlefs, Ivan Niell. "Design, simulation, manufacture and testing of a free-piston Stirling engine." PhD diss., Stellenbosch: Stellenbosch University, 2014.

[21] Joubert, L. H., J. Schutte, J. M. Strauss, and R. T. Dobson. "Design optimisation of a transverse flux, short stroke, linear generator." In *2012 XXth International Conference on Electrical Machines*, pp. 640-646. IEEE, 2012. https://doi.org/10.1109/ICEM20013.2012

[22] Aksoy, Fatih, and Can Cinar. "Thermodynamic analysis of a beta-type Stirling engine with rhombic drive mechanism." *Energy conversion and management* 75 (2013): 319-324. https://doi.org/10.1016/j.enconman.2013.06.043
[23] Shendage, D. J., S. B. Kedare, and S. L. Bapat. "An analysis of beta type Stirling engine with rhombic drive mechanism." *Renewable energy* 36, no. 1 (2011): 289-297. https://doi.org/10.1016/j.renene.2010.06.041
[24] Briggs, Maxwell H. "Improving power density of free-piston stirling engines." In *14th International Energy Conversion Engineering Conference*, p. 5016. 2016.
[25] Kumaravelu, Thavamalar, and Syamimi Saadon. "Heat transfer enhancement of a Stirling engine by using fins attachment in an energy recovery system." *Energy* 239 (2022): 121881. https://doi.org/10.1016/j.energy.2021.121881
[26] Afshari, Ebrahim, and Nasser Baharlou Houreh. "Performance analysis of a membrane humidifier containing porous metal foam as flow distributor in a PEM fuel cell system." *Energy conversion and management* 88 (2014): 612-621. https://doi.org/10.1016/j.enconman.2014.08.040
[27] Abidin, Mohamad Naufal Zainal, and Md Yushalify Misro. "Numerical Simulation of Heat Transfer using Finite Element Method." *Journal of Advanced Research in Fluid Mechanics and Thermal Sciences* 92, no. 2 (2022): 104-115. https://doi.org/10.37934/arfmts.92.2.104115
[28] Ben-Mansour, R., A. Abuelyamen, and Esmail MA Mokheimer. "CFD analysis of radiation impact on Stirling engine performance." *Energy conversion and management* 152 (2017): 354-365. https://doi.org/10.1016/j.enconman.2017.09.056
[29] Dol, Sharul Sham, Hiang Bin Chan, and Siaw Khur Wee. "FSI simulation of a flexible vortex generator and the effects of vortices to the heat transfer process." *Platform: A Journal of Engineering* 4, no. 2 (2020): 58-69.
[30] Dol, Sharul Sham, Hiang Bin Chan, Siaw Khur Wee, and Kumar Perumal. "The effects of flexible vortex generator on the wake structures for improving turbulence." In *IOP conference series: materials science and engineering*, vol. 715, no. 1, p. 012070. IOP Publishing, 2020. https://doi.org/10.1088/1757-899X/715/1/012070
[31] Dol, Sharul Sham, and Chan Hiang Bin. "Fluid-Structural Interaction Simulation of Vortices behind a Flexible Vortex Generator." In *2019 8th International Conference on Modeling Simulation and Applied Optimization (ICMSAO)*, pp. 1-5. IEEE, 2019. https://doi.org/10.1109/ICMSAO.2019.8880321
[32] Rebhi, Redha, Younes Menni, Giulio Lorenzini, and Hijaz Ahmad. "Forced-Convection Heat Transfer in Solar Collectors and Heat Exchangers: A Review." *Journal of Advanced Research in Applied Sciences and Engineering Technology* 26, no. 3 (2022): 1-15. https://doi.org/10.37934/araset.26.3.115
[33] Shlash, Bassam Amer Abdulameer, and Ibrahim Koç. "Turbulent fluid flow and heat transfer enhancement using novel Vortex Generator." *Journal of Advanced Research in Fluid Mechanics and Thermal Sciences* 96, no. 1 (2022): 36-52. https://doi.org/10.37934/arfmts.96.1.3652
[34] Chan, Hiang Bin, Tshun Howe Yong, Perumal Kumar, Siaw Khur Wee, and Sharul Sham Dol. "The numerical investigation on the effects of aspect ratio and cross-sectional shape on the wake structure behind a cantilever." *ARPN Journal of Engineering and Applied Sciences* 11, no. 16 (2016): 9922-9932.